ACS APPLIED MATERIALS & INTERFACES

www.acsami.org

Research Article

Ultralight, Structurally Stable Electrospun Sponges with Tailored Hydrophilicity as a Novel Material Platform

Jun Young Cheong, Mahsa Laghaei, Mathar Benker, Jian Zhu, Michael Mader, Chen Liang, Haoqing Hou, Seema Agarwal, Il-Doo Kim,* and Andreas Greiner*

Cite This: ACS Appl. Mater. Interfaces 2020, 12, 1800218011

Read Online

ACCESS | Metrics & More | Article Recommendations | Supporting Information

ABSTRACT: Sponges based on short electrospun fibers have received significant attention due to their ultrahigh porosity, lightweight, and multifunctional characteristics. In particular, polyimide (PI) sponges have been researched due to their exceptional mechanical properties and thermal stability. Nevertheless, a number of sponges, including PI, are usually hydrophobic and synthesized in toxic, nonwater solvents (e.g., 1,4-dioxane). Conversely, hydrophilic sponges disintegrate upon contact with water. Here, we suggest a new strategy to fabricate PI sponges in water by introducing a suitable surfactant, sodium dodecylbenzenesulfonate (SDBS) (sPI sponges). With less than 1 wt % of SDBS with respect to PI short fibers, they can be homogeneously dispersed in water and mixed well with poly(amic acid) (PAA) solution. The synthesized sponge, depending on the concentration of SDBS, showed hydrophilic properties and substantial water uptake above 5000%. The hydrophilic properties of the sponges, which are not common, and the preparation from aqueous solution introduc new research opportunities. Such hydrophilic sponges are particularly special because they do not swell in contact with water, wh makes them dimensionally stable. The methods presented here can serve as a milestone for the future development of various k of hydrophilic sponges applied for various applications, ranging from tissue engineering to oil/water separation.

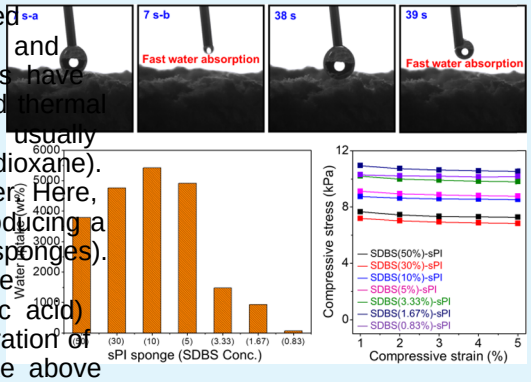

KEYWORDS: hydrophilic, PI, SDBS, electrospun sponge, water

1. INTRODUCTION

Recent advances in shorter techniques coupled with the versatility of polymer candidates have led to many significant progress in electrospun sponge research as novel open-cellular three-dimensional materials.[1] Conventionally, a number of polymeric sponges with low density and macroporosity have been reported[2,8] and have been applied in various applications, such as biomedical applications,[2] thermal insulation,[4] sound adsorption,[5] cancer vaccines,[6] and catalyst carriers.[7] Compared with polymeric sponges, electrospun sponges will be utilized in more diverse sets of applications attributed to their high porosity and tunable mechanical properties.[1] In particular, polyimide (PI) electrospun sponges have attracted considerable attraction due to their high macroporosity, thermal insulation, and excellent mechanical properties.[9,10] Applications of the PI range from micromachining technology to energy storage systems due to its versatile characteristics and morphologies.[11−17] Considering the additional application of electrospun fibers,[18−20] if various kinds of PI and other polymeric electrospun sponges can be fabricated, there will be significant progress.

Nevertheless, in view of practical manufacturing and mass production, the synthesis of PI sponges is hampered by several obstacles. First, conventional PI electrospun sponges are fabricated in a dioxane-based dispersion,[9,10] which is environmentally toxic and considerably expensive. Moreover, dispersing a poly(amic acid) (PAA) solution with fibers is difficult, as PAA solutions are made in the water solvent with a highly basic pH. After the imidization process, a number of PAA agglomerates can be seen within the PI sponges, which always remain a significant problem. Fabricating PI sponges in the water solvent can be an ideal solution to overcome all of these issues, but PI is very hydrophobic in nature and does not homogeneously disperse in water to form a high-quality sponge. Not only PI but other polymers that are hydrophobic also cannot be dispersed well in water, and this issue has hampered the practical use of electrospun polymeric sponges as feasible platforms for diverse applications. Moreover, these electrospun sponges are inherently hydrophobic. Hydrophilic electrospun sponges (such as PNIPAAM)[21] suffer from fluctuations in mechanical properties depending on pH and

Received: February 18, 2020
Accepted: March 11, 2020
Published: March 11, 2020

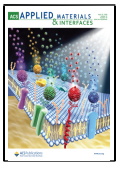

https://dx.doi.org/10.1021/acsami.0c03103
ACS Appl. Mater. Interfaces 2020, 12, 1800218011

Figure 1. (a) Schematic illustration of the synthesis of sPI sponges fabricated in DI water. Digital camera images of dispersion (b) before ultrasonication without SDBS, (c) after ultrasonication, and (d) after the addition of PAA. (e) Optical microscopy image and (f) distribution of the short PI fibers. (g and h) Digital camera image demonstrating the hydrophilic nature of the sPI sponge compared with the hydrophobic conventional PI sponge. The scale bars in (b), (c), and (d) are 10 mm, and the scale bar in e is 100 μm.

temperature and cannot be applied for various applications that require hydrophilicity and dimensional stability when in contact with water.

In this work, we suggest a highly feasible strategy not only to prepare electrospun polymeric sponges in water but also to fabricate hydrophilic PI sponges with SDBS (sPI sponge) by controlling the amount of sodium dodecylbenzenesulfonate (SDBS). The suggested approach does not require any additional processing but simply the addition of the desired amount of SDBS in water dispersion. Most importantly, this approach allows the preparation of hydrophilic sponges that are dimensionally stable in water (do not swell or disintegrate) without the need for cross-linking. This work demonstrated that less than 1 wt % of SDBS with respect to the short PI fibers is enough to fabricate sponges in water, whose hydrophilicity can be easily tuned by controlling the amount of SDBS. By tailoring this amount, a water uptake above 5000 wt % is viable, unprecedented for conventional hydrophobic sponges. The suggested method was further demonstrated for polyacrylonitrile (PAN) sponges, which show the versatility of the suggested method in this work. A myriad of applications have arisen from the fabrication of structurally stable polymeric sponges with tunable hydrophilicity and are expected to open up numerous opportunities in the near future, with numerous applications ranging from tissue engineering to oil/water separation.

2. MATERIALS AND METHODS

2.1. Materials. Electrospun polyimide (PI) nanofibers were provided by Jiangxi Xiancai Nanofibers Technology Co., Ltd., China. Ammonia (NH_3, 25 wt % in water) was purchased from Bernd Kraft. Sodium dodecylbenzenesulfonate (SDBS) was purchased from Sigma Aldrich. Poly(amic acid) (PAA) fiber was prepared according to a previous study.[9] PAN (M_n = 140 000) was purchased from Dolan.

2.2. Preparation and Dispersion of Short PI Fibers in Water with SDBS. The preparation of short PI fibers is similar to that reported in the previous literature.[9] In brief, 20 g of electrospun PI nanofibers was cut into small pieces and mixed with 2 g of solution consisting of water/dioxane (50:50 v/v). The mixture was frozen with liquid nitrogen until it became solid. Then, the cooled mixture was cut by a mixer (Robot Coupe Blixer 4, Rudolf Lange GmbH & Co. KG) at 3500 rpm for 2 min to be made into short fibers. The short fibers were then filtered using vacuum filtration and dried for one day. The dried short PI fibers (0.06 g unless otherwise stated) were then dispersed again in 6 g of distilled water with different concentrations of SDBS. The PI fiber dispersions were ultrasonicated for 30 min and formed a homogenous suspension.

2.3. Preparation of PAA Solution and Combination with Short PI Fiber Dispersion. The PAA solution was prepared in water as follows: 200 mg of PAA fiber was mixed into 10 g of a solution consisting of 0.3 g of NH_3 and 9.7 g of distilled water. The solution was stirred at 410 rpm for 10 min, after which it was completely dissolved. Prior to the injection of the PAA solution into the short PI fiber dispersion, 2 drops of NH_3 were placed onto the short PI fiber dispersion. The PAA solution was mixed with the short PI fiber dispersion, and the final solution was ultrasonicated for 30 min to allow the homogeneous dispersion of PAA into PI.

2.4. Preparation of sPI Sponges. The PAA/PI composite solution was placed into an uncapped glass vial (approximately 10 mL). The glass vial was placed into ethanol, and liquid nitrogen was used to lower the temperature of ethanol to below −20 °C. When the solution became completely solid, it was dried by a freeze-dryer (Firma Christ Osterode, 2-16) for 2 days under 0.03 mbar. The imidization process consisted of four steps. First, the vacuum was injected into the tube furnace. Next, the dried PAA/PI composite was heated to 150 °C for 1 h. The temperature was then raised to 280 °C

https://dx.doi.org/10.1021/acsami.0c03103
ACS Appl. Mater. Interfaces 2020, 12, 18002−18011

and heated for an additional 2 h. Finally, the sample was cooled and removed from the tube furnace when the temperature reached 20 °C.

2.5. Preparation of PAN Sponges with SDBS. For the fabrication of PAN nanofibers, 6 g of PAN was dissolved in 50 g of dimethylformamide (DMF) and stirred for 24 h at 300 rpm. Then, the PAN nanofibers were electrospun under the following conditions: 20 cm between the tip of the syringe and the collector, 17.5 kV applied voltage, 1 mL h^{-1} flow rate, and 23 G gauge needle. After electrospinning, the PAN nanofibers were cut into short PAN fibers with water using a high-shear mixer. The density of the short PAN fiber dispersion was 3.6 mg cm^{-3}, and SDBS was added to reach the 10 wt % concentration with respect to the short PAN fiber. For the fabrication of the PAN sponge, the PAA solution was also added in the same ratio as that used for fabricating the PI sponge. After drying with the freeze-dryer, the same imidization step was then adopted to fabricate the PAN sponge.

2.6. Preparation of Bacteria and Characterization of Biofilms. The *Escherichia coli* (DSMZ Braunschweig) were harvested in a nutrient medium of peptone (Fulka) and a mixture of meat extract (LB culture medium) (Roth) in extra pure water provided by a Milli-Q Plus system (conductivity = 0.055 Ω cm^{-1}, pH = 7) at 37 °C for 24 h. The *E. coli* pellet was centrifuged and washed with water, followed by filtration with various PI sponges. Bacteria survival assessment and colony counting were conducted by agar plate tests and a series of dilution experiments. The growth of white colonies revealed the presence of bacteria with biological activities. The agar plates were prepared by mixing 15 g of LB culture medium (Roth) and 12 g of agar-agar (Roth) in 750 mL of water. Biofilm formation was tested with a confocal laser microscope via staining cells with Syto9 (green-fluorescent nucleic acid stain) (Sigma Aldrich).

2.7. Various Characterization. For calculating the short fiber length distribution, an optical microscope (KEYENCE VH-Z500) was used to capture the images of the short PI fibers and calculate their lengths. To delve into the morphologies of electrospun sponges and fibers, a scanning electron microscope (SEM) (Zeiss Leo 1530) was used. The morphology of the short fiber was further visualized by a transmission electron microscope (TEM) (Zeiss CEM902) operating at 80 kV. To measure the hydrophilic/hydrophobic properties, contact angle analysis was conducted by placing a 5 μL drop of water into the electrospun sponges and visualizing each sponge using the Drop Shape Analyzer (KSV Advance, v1.3.1) and Milli-Q water. Water uptake was examined by measuring the amount of water absorbed by the sponge after 5 min of immersion in water and measuring the weight of the sponge before and after water immersion. The density of the sPI sponges was calculated by measuring the weight of the sponge, calculating its volume by measuring each side, and dividing the weight by volume. The compressive stress−strain curves were conducted at a strain of 50% with a compression speed of 4 mm min^{-1} using a mechanical tester with DIN 53 421 (load sensor of 200 N, compression speed of 5 mm min^{-1}, room temperature). The confocal microscopy conditions were set as a minimum of 15, a maximum of 200, and an opacity of 30. The chemical states of PI and SDBS were further probed by X-ray photoelectron spectroscopy (XPS, Sigma Probe, Thermo VG Scientific).

3. RESULTS AND DISCUSSION

The fabrication procedure of the hydrophilic sPI sponges used water as the solvent (Figure 1), unlike the previous methods, which suggested fabricating PI sponges in dioxane.[9,10] The scanning electron microscopy (SEM) images of pristine PI nanofibers and PAA (Figure S1) clearly show the one-dimensional nanofibrous structure of PI. After sectioning the long electrospun PI nanofibers into short PI fibers using a high-shear mixer, they were initially mixed in water without SDBS (Figure 1b), where they were not dispersed well. However, after the addition of SDBS and the ultrasonication step, the short PI fibers were well dispersed in water (Figure 1c), and some bubbles formed from the introduction of SDBS.[22] This bubble formation is a common phenomenon and is a thermodynamically favorable process due to the amphiphilic nature of SDBS. In addition to the PI dispersion, a PAA solution was also prepared (Figure S2) in aqueous solution. As both the PI dispersion and PAA solution were in aqueous solution, the short PI fibers were dispersed well even after the addition of the PAA solution (Figure 1d).

Notably, the addition of dissolved PAA to the dispersion of short PI nanofibers is crucial for the preparation of PI sponges with exceptional mechanical properties. Based on previous literature studies,[9,10,23] PAA helps to act as a binder to create junctions between short PI fibers, which are critical to the compressible characteristics of PI electrospun sponges. To further characterize the dispersion of short PI fibers in water, optical microscopy was conducted (Figure 1e) and clearly showed that short PI fibers were dispersed well in the water solvent with the addition of SDBS. The fiber length distribution (Figure 1f) indicates that a substantial number of short PI fibers in the range of 200−600 μm were made, the distribution of which was similar to what was previously reported.[9] The transmission electron microscopy (TEM) image of the short PI fibers (Figure S3) exhibits a polymeric nanofibrous structure. When SDBS was introduced into the PI short fibers, the imidization temperature played a critical role in the overall fabrication of sPI sponges. At low imidization temperatures (230 °C) (Figure S4), some sPI sponges were crumbled and underwent cracking, whereas sPI sponges fabricated at high imidization temperatures (280 °C) retained good structural stability. Based on previous literature studies,[9,10,23] different temperatures (from 240 to 350 °C) were used to fabricate suitable PI-based electrospun sponges. Generally, imidization at low temperature could prevent the thermal shrinkage of the PI sponge,[23] while imidization at high temperatures[9,10] could result in a mechanically stable PI sponge. The introduction of SDBS in sPI sponges resulted in a suitable imidization temperature of 280 °C, which is in the range of the temperatures mentioned in the previous studies.[9,10,23] As a result, various physicochemical properties of sPI sponges, fabricated at 280 °C, were examined. These sponges were initially fabricated by controlling the weight ratio between surfactant and short fiber weight ratio (50, 30, 10, 5, 3.33, 1.67, and 0.83 wt % with respect to PI denoted as SDBS(50%)-sPI, SDBS(30%)-sPI, SDBS(10%)-sPI, SDBS(5%)-sPI, SDBS(3.33%)-sPI, SDBS(1.67%)-sPI, SDBS(0.83%)-sPI, and SDBS(50%)-sPI sponge), while the amounts of the solvent and short PI were held constant. The SEM images of PI sponges with different concentrations of SDBS are shown in Figure S5, where the formation of a microsheet-like morphology is shown, different from that of the conventional PI sponges.[9,10] This is attributed to the presence of precipitated SDBS that is attached to the network of short PI fiber and PAA, which helps to interact with water through its hydrophilic group.[24] To examine the elemental distribution of SDBS, the overall SEM-energy-dispersive X-ray spectroscopy (SEM-EDX) mapping of C, O, Na, S, and Pt (Figure S6) and that for Na and S combined were conducted, which are key elements for indicating SDBS (Figure S7). For the parts that have a number of microsheets, the overall intensity of SDBS is evident, suggesting that a number of these microsheets are formed as a result of SDBS introduction. In contrast, the previously reported PI sponges[9,10] did not have this microsheet morphology. X-ray photoelectron spectroscopy (XPS) analysis (Figure S8) was further carried out to

https://dx.doi.org/10.1021/acsami.0c03103
ACS Appl. Mater. Interfaces 2020, 12, 18002−18011

Figure 2. Contact angle analysis for different sPI sponges with (a) broad range of SDBS concentrations and (b) SDBS concentrations below the critical concentration (concentration at which transition from hydrophilic to hydrophobic properties takes place). Water uptake test of (c) different sPI sponges and (d) SDBS(10%)-sPI sponge with different densities. Water uptake cycles of (e) different sPI sponges and (f) SDBS(10%)-sPI sponge with different densities.

understand whether the introduction of SDBS resulted in significant changes in the chemical states of respective elements. XPS analysis of C, O, and Na was conducted, and it was verified that no significant changes took place, except for the emergence of new peaks for Na, which is ascribed to Na−O bonds.[25,26] The introduction of SDBS not only resulted in morphological transitions but also significantly altered hydrophobic/hydrophilic properties. These dynamic changes can be visually observed macroscopically by simply injecting a drop of water onto the conventional PI sponge and prepared sPI sponges (Figure 1g,h). Unlike the conventional PI sponge, which forms a hydrophobic contact angle with the water droplet, the prepared sPI sponges simply absorb water, which is unprecedented, given the original chemical properties of pristine PI.

As seen in Figure 1h, the prepared sPI sponges show significantly different properties, particularly in their hydrophilicity. Conventionally, the synthesized PI sponges exhibit rather hydrophobic properties, as seen from the contact angles of the PI sponges fabricated in dioxane (Figure S9). Before delving into more details, contact angle analysis of the prepared sPI sponges (Figure 1h was conducted in a real-time movie, which consistently shows that the water can just be placed dropwise into the sponges upon contact (Figure S10 and Movie S1). This phenomenon is very unusual and needs to be examined in more detail. To analyze the contact angle data, various sPI sponges were fabricated. Then, each of these sPI sponges was tested for contact angle analysis, and the dynamics of their interactions with water were visualized in real time (Movies S2S8). Surprisingly, a majority of the sPI sponges exhibited complete water wetting and absorbed water instantaneously (less than 100 ms) without forming any PI contact with water. The average water contact angle of different sPI sponges (Figure 2a) further corroborates two important characteristics that need to be discussed. First, there is a critical concentration at which water is not absorbed into the sponge, suggesting that an SDBS concentration less than 1 wt % allows the contact angle of water, rather than simple adsorption. This finding can be further attributed to the loading amount of SDBS, where an obviously decreasing amount of SDBS in the sPI sponges with less SDBS in the suspension causes the sponge to be less hydrophilic, as can be indirectly inferred from the EDX composition analysis for Na and S that are related to SDBS (Figure S11), where less surfactant was loaded onto sPI sponges at lower concentrations. For the SDBS(0.83%)-sPI sponge, the contact angle

https://dx.doi.org/10.1021/acsami.0c03103
ACS Appl. Mater. Interfaces 2020, 12, 18002−18011

Figure 3.(a) Calculated density, (b) compressive stress−strain curve, and (c) compressive cycle tests of different sPI sponges.

of water was found to be approximately 1,100%, which is slightly hydrophobic. Furthermore, for the SDBS(50%)-sPI sponge and the SDBS(1.67%)-sPI sponge, a hydrophilic surface was maintained, regardless of the amount of SDBS used. Therefore, a relatively low loading amount of SDBS (even less than 2.0 wt %) may be enough to induce hydrophilic surface properties. To further explore the effect of SDBS concentration on the contact angles, sPI sponges with different loading amounts of SDBS (1.5 and 1.17 wt %) were fabricated and tested for contact angle analysis. As the objective of this study was to investigate hydrophilic properties, SDBS concentrations lower than 0.83 wt % were not considered. The contact angles were further probed for the critical concentration of SDBS (Figure 2b). At an SDBS concentration of 1.5 wt %, the average contact angle was 71.7° and increased to 87.5 and 110° when the concentration was decreased to 1.17 and 0.83 wt %, respectively. The wide error bars for SDBS concentrations of 1.5 and 1.17 wt % can be attributed to the variance in hydrophilicity, which is dependent on the presence of SDBS. In consideration of contact angle, surface tension is also an important factor, as the contact angle is related to surface tension based on the following equation: $_s = _{sl} + _l \cos$, where $_s$ is the surface free energy of the solid, $_{sl}$ is the interfacial tension between liquid and solid, and $_l$ is the surface tension of the liquid. When the contact angle is 0, it is evident that $_s = _{sl} + _l$. For the case of SDBS(0.83%)-sPI, $= _{sl} 0.34 _l$, where the overall surface free energy of the solid is smaller. As water uptake is the typical characteristic of hydrophilic polymers,[27] the water uptake of sPI sponges with identical concentrations of SDBS, as shown in Figure 2a, was further tested (Figure 2c). The sponges were cut with similar dimensions (circle with a radius of 0.8 cm) (Figure S12), and the weight changes of the sPI sponges before and after water uptake were calculated. Contrary to common knowledge that a higher loading amount of surfactant results in higher water uptake, the water uptake was actually highest for the SDBS(10%)-sPI sponge. For the SDBS(10%)-sPI sponge, the initial water uptake was above 5000 wt %, despite the intrinsic hydrophobic nature of PI. Surprisingly, the water uptake for the SDBS(5%)-sPI sponge was higher than that of the SDBS(30%)-sPI sponge. This phenomenon can be attributed to the optimal decoration of SDBS within the PI sponge network in the freeze-drying process at high SDBS concentrations (30−50 wt %). SDBS has a high tendency to agglomerate with each other, whereas at relatively lower SDBS concentrations (5−10 wt %), SDBS is more uniformly decorated, leading to optimized water uptake properties. Furthermore, even for the SDBS(0.83%)-sPI sponge, the weight increased by 74 wt %, which can be attributed to the ultra-porous structure that allows a substantial amount of water to be adsorbed, despite the high water contact angle. As the SDBS(10%)-sPI sponge showed the optimal water uptake, it was further examined by varying the densities of the fabricated SDBS(10%)-sPI sponge. The amount of water was fixed, whereas the amount of short PI fibers was adjusted to 0.03, 0.045, and 0.075 g, with adjusted amounts of SDBS, which resulted in different densities of sponges. Overall, the water uptake was inversely proportional to the density (Figure 2d), and low density led to high water uptake, as much as 3400 wt %. The calculated density of all sPI sponges with different amounts of short PI fibers was higher than the theoretical density because the fibers shrank during the freeze-drying process. To examine the consistency in water uptake, the water uptake of different PI sponges (Figure 2e) and the SDBS(10%)-sPI sponge with different densities (Figure 2f) was further examined for three cycles. SDBS(10%)-sPI (0.03), SDBS(10%)-sPI (0.045), SDBS(10%)-sPI (0.06), and SDBS(10%)-sPI (0.075) exhibit water uptake retention of 92.7, 107.2, 83.2, and 99.9%. Although slight variances are present from one cycle to another, the water uptake shows consistent trends, where sPI sponges consistently exhibit considerable water uptake, which is rarely a characteristic of conventionally manufactured hydrophobic electrospun sponges. For visual demonstration, the SDBS(1%)-sPI sponge was compared with a conventional PI sponge on water (Figure S13). Clearly, the SDBS(1%)-sPI sponge does not float on water, unlike the conventional PI sponge, which is due to the different water uptake properties of the two types of sponges.

In addition to the hydrophilic and water uptake properties, the mechanical properties of the hydrophilic sPI sponge are also important parameters for determining the quality of sponges, as elucidated in previous studies.[9,10,28] As shown (Movie S9), the hydrophilic sPI sponge is reversibly compressible underwater. Other hydrophilic sponges, such as poly(N-isopropylacrylamide) (PNIPAM) sponges, are not reversibly compressible underwater and are not dimensionally stable, which makes handling wet sponges very difficult.[24] This problem has been resolved by sPI sponges. First, the most important mechanical property to be examined for polymeric sponges is compressive stress, which is affected by a number of parameters, such as the junction between sheets, bulk density, and porosity. Density is the most important parameter, as compressive forces are most directly proportional to the given densities;[28] the higher the density is, the stronger the compressive stress is. Because most electrospun sponges undergo volume shrinkage upon freeze-drying, their actual density after heat treatment needs to be investigated. The calculated densities of sPI sponges with different concen-

https://dx.doi.org/10.1021/acsami.0c03103
ACS Appl. Mater. Interfaces 2020, 12, 18002−18011

Figure 4.(a) SEM image of electrospun PAN nanobers. (b) Fiber length distribution of the short PAN bers. (c) Digital camera image of an electrospun PAN sponge exhibiting hydrophilic properties. (d) Water adsorption properties (in real time) of electrospun PAN sponges. The scale bar in (a) is 4 m.

trations of SDBS (Figure 3a) show two important trends, which are denoted as the "critical point of stability" and the "water uptake critical point". In addition to the water uptake critical point, which was previously described in Figure 2a, another important threshold concentration appeared. Overall, the calculated densities of the sPI sponges were relatively larger (14 20 mg mL^{-1}) than the original density (10 mg mL^{-1}) due to the volume shrinkage that occurred in the freeze-drying process and subsequent heat treatment. Interestingly, from the SDBS(30%)-sPI sponge to the SDBS(1.67%)-sPI sponge, the density steadily increases, which is contrary to the previous notion that the addition of surfactants will lead to lower densities. This phenomenon can be explained as follows: with more loading of surfactants, the short bers can be easily disconnected, and the microsheets derived from the surfactants can create more macropores, which lead to lower densities. SDBS has a density of 1 g mL^{-1}, which is much higher than that of the short PI ber, as evidenced by the heating of conventional PI bers in the water solvent; therefore, the density of all PI sponges with SDBS is higher than that of the conventional PI sponge. The effect of SDBS becomes minimal for the SDBS(0.83%)-sPI sponge, where the density is slightly lower than the SDBS(1.67%)-sPI sponge. Based on the densities of respective sPI sponges, porosity (P(%)) can be calculated based on the equation $P(\%) = (1 - \rho_{PI,s}/\rho_{PI,b}) \times 100$, where $\rho_{PI,s}$ is the density of the electrospun PI sponge and $\rho_{PI,b}$ is the density of the bulk PI (1.4 g cm^{-3}). The trends for density in Figure 3a show a direct correlation to the compressive stress in the initial cycle for each PI sponge (Figure 3b), as a larger density usually leads to a higher compressive strain. A slight deviation is shown for the SDBS(50%)-sPI sponge, where the compressive strain is smaller than that for the SDBS(10%)-sPI sponge. This trend can be attributed to the fact that too much loading of SDBS leads to the unstable formation of junctions between the short PI bers and short PI bers/microsheets, where structural stability cannot be guaranteed. This phenomenon is precisely the reason that a critical point of stability exists (Figure 3a). The compressive strain curves for sPI sponges with different concentrations of SDBS shown in Figure 3b exhibit outstanding mechanical properties compared with those of the conventional PI sponge fabricated in dioxane (Figure S14). To further investigate the changes in maximum compressive strains with respect to the cycles, the maximum compressive stress for different sPI sponges was plotted and analyzed for over cycles (Figures S15 and 3c). All of the sPI sponges underwent a 5% or less decrease in maximum compressive stress, which highlights the structural integrity of PI sponges combined with SDBS. In particular, for SDBS(10%)-sPI sponge-7, a less than 4% decrease in maximum compressive stress occurred, showing the maintenance of strong mechanical strength. Another SDBS(20%)-sPI sponge was fabricated and tested for simple mechanical compression and visualized after 10 and 100 cycles (Figure S16), and the original structure of the PI sponges was well maintained even after 100 repetitive cycles of bending. All of the results presented above guarantee the mechanical stability of the sPI sponges.

To demonstrate the universality of this approach, the same synthetic strategy was extended to polyacrylonitrile (PAN). An SDBS concentration of 10 wt % for PI sponges (0.006 g of SDBS in 6 g of water) was chosen as the standard concentration to fabricate electrospun PAN sponges in the water solvent. Initially, the PAN nanobers were fabricated by electrospinning (Figure 4a), cut into short bers in water, and mixed with the PAA solution and SDBS (Figure S17). For PAN, the PAA solution was further added, and the dispersion was still stable. The short PAN bers have a wide range of length distribution compared with that of the short PI bers (Figure 4b). The PAN dispersion underwent freeze-drying and subsequent heat treatment and formed electrospun sponges. These fabricated sponges also exhibit hydrophilic properties with normal sponge shapes (Figure 4c). The SEM images of the electrospun PAN sponges (Figure S18) show that the formation of microsheets is also visible. The density of the electrospun PAN sponge was calculated to be 5.7 mg cm^{-3}, which is significantly lower than that of the PI electrospun sponge. However, despite such low density, the fabricated electrospun PAN sponges exhibited highly hydrophilic properties (Figure 4d), where a similar water adsorption phenomenon was obvious based on the video (Movie S10). Finally,

https://dx.doi.org/10.1021/acsami.0c03103
ACS Appl. Mater. Interfaces 2020, 12, 18007 18011

cyclic bending tests (Figure S19) were conducted by pressing the PAN sponges for 100 cycles, and the overall structural integrity was maintained.

To verify the hydrophilic properties of the sPI sponge, we investigated the interaction of the sponges with bacterial suspensions. The potential use of hydrophilic sponges as biofilm substrates is critical among various applications, such as microbial fuel cells, which are not possible with the state-of-the-art hydrophobic versions of PI sponges. The formation of artificially triggered biofilms is currently the major challenge in developing microbial fuel cells.[29] Microorganisms are capable of multiplying and reproducing themselves by forming colonies called biofilms. The production of biofilms exclusively demands the attachment of colonies to the surfaces. An important factor for this step is that the properties of the surface need to be adjusted for the suitable attachment of colonies. As an example of adjustable properties, the production of hydrophilic sponges introduces new opportunities in the field of microbial fuel cells. Microbial fuel cells continuously convert biological oxidation processes into electrical energy,[30,31] which can overcome the drawbacks of fuel cells, such as by providing hydrogen for chemical energy. The SDBS(50%)-sPI sponge, SDBS(10%)-sPI sponge, and SDBS(3.33%)-sPI sponge, as well as conventional PI sponges, were inserted between plastic tubes (Figure S20). A 0.5 g suspension of *E. coli* containing two different dyes (green for live *E. coli* and blue for dead *E. coli*) with 10^{14} CFU mL^{-1} of *E. coli* colonies was placed dropwise onto each of the electrospun sponges and kept for just 1 min to examine the effect of hydrophilicity in terms of efficiently infiltrating *E. coli*. Within 1 min, all of the hydrophilic PI sponges absorbed the *E. coli* suspension, without any suspension leaving the electrospun sponges, whereas the suspension stayed on top of the hydrophobic PI sponge. This result is reasonable because the weight of the hydrophilic PI sponges ranged from 0.2 to 0.3 g, and all of the PI sponges with the above surfactant concentrations adsorbed a considerable amount of water (from approximately 1000 to 5000 wt %). After *E. coli* infiltration, confocal microscopy analysis was carried out by converting the pristine optical microscopy image into confocal microscopy images (Figure 5a−d) for the conventional hydrophobic PI sponge and the SDBS(50%)-sPI sponge, SDBS(10%)-sPI sponge, and SDBS(3.33%)-sPI sponge. In contrast to the conventional hydrophobic PI sponge, which does not show any presence of live *E. coli* (Figure 5a), all of the sPI sponges exhibit the presence of live *E. coli* (Figure 5b−d). The presence of *E. coli* is less predominant for the SDBS(3.33%)-sPI sponge, which can be attributed to the slow adsorption of the *E. coli* suspension. Interestingly, the *E. coli* not only adsorbed well on the hydrophilic PI sponges but also started creating more colonies and transformed the electrospun sponge into biofilms. The SEM images of the SDBS(50%)-sPI sponge (Figure S21a) after one (Figure S21b) and four weeks (Figure S21c) demonstrate the steady process of *E. coli* adsorption, the creation of more *E. coli* colonies, and the formation of biofilms, which are unprecedented for hydrophobic PI sponges.

Finally, a number of applications could either originate from or be derived from hydrophilic polymeric sponges. The schematic illustration of various applications that are related to hydrophilic electrospun sponges is showcased in Figure S22. The need for developing hydrophilic sponges is crucial because they could be used for various applications ranging from wastewater treatment to tissue engineering. For instance, wettability in an aqueous solution could be a critical factor to boost the electrochemical performance,[32] and a hydrophilic polymer can even be used as active electrode materials for rechargeable devices.[33] Hydrophilic sponges could also be used for wastewater treatment,[34] where hydrophilic properties are crucial for contacting with water. Additionally, hydrophilic properties can be crucial in the generation of water vapor.[35] In particular, for hydrophilic materials with high macroporosity, such as sponges, there could be a number of sites where water vapor can be generated. This further supports the potential application of generating electricity by coating carbon substances with polymers because a recently published work[36] showed that evaporation-induced electricity generation is possible with hydrophilic nanostructured carbon materials. The development of hydrophilic sponges is also crucial for tissue engineering,[37] as biological responses and cellular attachment are directly dependent on hydrophilic nature. Additionally, as a well-known application, the hydrophilic polymeric sponge could be an ideal material to be used as a component of oil/water separation.[38,39] Based on these records, there is a need to develop various types of hydrophilic electrospun sponges with considerable mechanical properties at different temperatures/pH that could be utilized for many of these applications in a scalable and eco-friendly manner.

Figure 5. Optical microscopy image of (a) conventional hydrophobic PI sponges and (b) SDBS(50%)-sPI sponge, (c) SDBS(10%)-sPI sponge, and (d) SDBS(3.33%)-sPI sponge. Agar plate test images of (e) conventional hydrophobic PI sponge and (f) SDBS(50%)-sPI sponge after four weeks in the nutrient medium. The presence of white colonies confirms the presence of *E. coli* in the SDBS(50%)-sPI sponge after four weeks (scale bars (a): 0.2 mm; (b, c, and d): 0.5 mm).

https://dx.doi.org/10.1021/acsami.0c03103
ACS Appl. Mater. Interfaces 2020, 12, 18002−18011

4. CONCLUSIONS

We first proposed a universal method for not only fabricating hydrophobic electrospun sponges in water but also tuning the hydrophilicity of fabricated electrospun sponges simply by introducing a suitable surfactant (SDBS). Even for the SDBS(1.67%)-sPI sponge, the electrospun sponge readily absorbed water without forming contact angles. Moreover, for the SDBS(10%)-sPI sponge, it demonstrated a significant water uptake of above 5000 wt %, which could be as high as 8000 wt % when the density was reduced to form more macropores. In addition to exhibiting hydrophilicity, the fabricated sPI sponge also exhibited outstanding mechanical properties not only in its pristine state but also when in contact with water under different pH values and temperatures and can be broadly utilized for diverse applications. Furthermore, the suggested approach can be applied to fabricate other naturally hydrophobic polymeric sponges, such as PAN, in water and transform their hydrophobic characteristics into hydrophilic characteristics. The fabricated sPI sponge exhibits stable adsorption, which allows it to be transformed into an ionic. Without sacrificing the intrinsic material properties of the electrospun sponges, this work establishes a demonstration on how to manufacture hydrophilic electrospun sponges, which are expected to be applied to various fields of research and industry.

ASSOCIATED CONTENT

* Supporting Information

The Supporting Information is available free of charge at https://pubs.acs.org/doi/10.1021/acsami.0c03103.

SEM images of pure PI nanofiber and PAA nanofiber (Figure S1); Digital camera images of PI short fiber dispersion and PAA solution (Figure S2); TEM image of PI short fibers (Figure S3); Digital camera images of PI sponges fabricated at the heat treatment temperature of 230 °C with different surfactant loading amount (Figure S4); SEM images of various sPI sponges (Figure S5); SEM-EDS mapping of sPI sponges according to various kinds of elements (Figure S6); SEM-EDS mapping of Na and S (components of SDBS) on sPI sponges (Figure S7); XPS analysis of conventional PI sponge and SDBS(5%)-sPI sponge (Figure S8); Contact angle analysis of conventional PI sponges (Figure S9); In situ microscopy snapshots of the contact angle analysis of sPI sponges (Figure S10); Weight percent of Na and S with respect to the concentration of SDBS (Figure S11); Digital camera images of various sPI sponges (Figure S12); Digital camera images of conventional PI sponge and sPI sponge (Figure S13); Compressive stress-strain curves for pristine PI sponges in the 1st cycle and cyclic compressive stress-strain curves of pristine PI sponges (Figure S14); Cyclic compressive stress-strain curves of various sPI sponges (Figure S15); Cyclic bending tests of sPI sponges (Figure S16); Digital camera images of dispersed PAN short fibers in water with SDBS and PAA solution (Figure S17); SEM images of fabricated PAN sponges with SDBS (Figure S18); Mechanical bending tests for PAN electrospun sponges (Figure S19); Digital camera images of bacterial adhesion test set-ups for sPI sponges (Figure S20); SEM images of SDBS(50%)-sPI sponge showing the structural degradation after bacterial absorption (Figure S21); Schematic illustration of potential applications of hydrophilic electrospun sponges (Figure S22) (PDF)

Water adsorption of the sPI sponge (x4 faster) (Movie S1) (AVI)

Contact angle analysis of the SDBS(50%)-sPI sponge (x4 faster) (Movie S2) (AVI)

Contact angle analysis of the SDBS(30%)-sPI sponge (x4 faster) (Movie S3) (AVI)

Contact angle analysis of the SDBS(10%)-sPI sponge (x4 faster) (Movie S4) (AVI)

Contact angle analysis of the SDBS(5%)-sPI sponge (x4 faster) (Movie S5) (AVI)

Contact angle analysis of the SDBS(3.33%)-sPI sponge (x4 faster) (Movie S6) (AVI)

Contact angle analysis of the SDBS(1.67)-sPI sponge (x4 faster) (Movie S7) (AVI)

Contact angle analysis of the SDBS(0.83%)-sPI sponge (x4 faster) (Movie S8) (AVI)

Mechanical stability of the sPI sponge (x4 faster) (Movie S9) (AVI)

Contact angle analysis of the hydrophilic PAN sponge (x4 faster) (Movie S10) (AVI)

AUTHOR INFORMATION

Corresponding Authors

Il-Doo Kim – Department of Materials Science and Engineering, Korea Advanced Institute of Science and Technology (KAIST), Daejeon 34141, Republic of Korea; orcid.org/0000-0002-9970-2218; Email: idkim@kaist.ac.kr

Andreas Greiner – Macromolecular Chemistry and Bavarian Polymer Institute, University of Bayreuth, Bayreuth 95440, Germany; orcid.org/0000-0002-5310-3850; Email: greiner@uni-bayreuth.de

Authors

Jun Young Cheong – Department of Materials Science and Engineering, Korea Advanced Institute of Science and Technology (KAIST), Daejeon 34141, Republic of Korea

Mahsa Ma – Macromolecular Chemistry and Bavarian Polymer Institute, University of Bayreuth, Bayreuth 95440, Germany

Lothar Benker – Macromolecular Chemistry and Bavarian Polymer Institute, University of Bayreuth, Bayreuth 95440, Germany

Jian Zhu – Macromolecular Chemistry and Bavarian Polymer Institute, University of Bayreuth, Bayreuth 95440, Germany

Michael Mader – Macromolecular Chemistry and Bavarian Polymer Institute, University of Bayreuth, Bayreuth 95440, Germany

Chen Liang – Macromolecular Chemistry and Bavarian Polymer Institute, University of Bayreuth, Bayreuth 95440, Germany

Haoqing Hou – Department of Chemistry and Chemical Engineering, Jiangxi Normal University, Nanchang 330022, China

Seema Agarwal – Macromolecular Chemistry and Bavarian Polymer Institute, University of Bayreuth, Bayreuth 95440, Germany; orcid.org/0000-0002-3174-3152

Complete contact information is available at: https://pubs.acs.org/10.1021/acsami.0c03103

Notes

The authors declare no competing financial interest.

ACKNOWLEDGMENTS

This work was supported by the National Research Foundation of Korea (NRF) (grant no. 2014R1A4A1003712 (BRL Program)), the Wearable Platform Materials Technology Center (WMC) funded by the NRF grant of the Korean government (MSIP) (no. 2016R1A5A1009926), the NRF, and a grant funded by the Korean government (NRF-2017H1A2A1042006-Global Ph.D. Fellowship Program). Support by DFG is kindly acknowledged.

REFERENCES

(1) Jiang, S.; Agarwal, S.; Greiner, A. Low-Density Open Cellular Sponges as Functional Materials. Angew. Chem., Int. Ed. 2017, 56, 15520 15538.

(2) Singhal, P.; Small, W.; Cosgriff-Hernandez, E.; Maitland, D. J.; Wilson, T. S. Low density biodegradable shape memory polyurethane foams for embolic biomedical applications. Acta Biomater. 2014, 10, 67 76.

(3) Okolieocha, C.; Beckert, F.; Herling, M.; Breu, J.; Mülhaupt, R.; Altstädt, V. Preparation of microcellular low-density PMMA nanocomposite foams: Influence of different fillers on the mechanical, rheological and cell morphological properties. Compos. Sci. Technol. 2015, 118, 108 116.

(4) Lee, J.; Chang, J. Y. Preparation of a compressible and hierarchically porous polyimide sponge via the sol gel process of an aliphatic tetracarboxylic dianhydride and an aromatic triamine. Chem. Commun. 2016, 52, 10419 10422.

(5) Si, Y.; Yu, J.; Tang, X.; Ge, J.; Ding, B. Ultralight nanofibre-assembled cellular aerogels with superelasticity and multifunctionality. Nat. Commun. 2014, 5, No. 5802.

(6) Bencherif, S. A.; Sands, R. W.; Ali, O. A.; Li, W. A.; Lewin, S. A.; Brashler, T. M.; Shih, T.-Y.; Verbeke, C. S.; Bhatta, D.; Dranoff, G.; Mooney, D. J. Injectable cryogel-based whole-cell cancer vaccines. Nat. Commun. 2015, 6, No. 7556.

(7) Duan, G.; K-Serrano, M.; Greiner, A. Highly Efficient Reusable Sponge-Type Catalyst Carriers Based on Short Electrospun Fibers. Macromol. Rapid Commun. 2017, 38, No. 1600511.

(8) Deuber, F.; Mousavi, S.; Hofer, M.; Adlhart, C. Tailoring Pore Structure of Ultralight Electrospun Sponges by Solid Templating. ChemistrySelect 2016, 1, 5595 5598.

(9) Jiang, S.; Uch, B.; Agarwal, S.; Greiner, A. Ultralight, Thermally Insulating, Compressible Polyimide Fiber Assembled Sponges. ACS Appl. Mater. Interfaces 2017, 9, 32308 32315.

(10) Jiang, S.; Reich, S.; Uch, B.; Hu, P.; Agarwal, S.; Greiner, A. Exploration of the Electrical Conductivity of Double-Network Silver Nanowires/Polyimide Porous Low-Density Compressible Sponges. ACS Appl. Mater. Interfaces 2017, 9, 34286 34293.

(11) Srinivasan, R.; Baren, B.; Dreyfus, R. W. Ultraviolet laser ablation of polyimide films. J. Appl. Phys. 1987, 61, 372.

(12) Harasimowicz, M.; Orluk, P.; Zakrzewska-Trznadel, G.; Chmielewski, A. G. Application of polyimide membranes for biogas purification and enrichment. J. Hazard. Mater. 2007, 144, 698 702.

(13) Frazier, A. B. Recent applications of polyimide to micromachining technology. IEEE Trans. Ind. Electron. 1995, 42, 442 448.

(14) Lee, J.; Lee, C.-L.; Park, K.; Kim, I.-D. Synthesis of an Al_2O_3 coated polyimide nanofiber mat and its electrochemical characteristics as a separator for lithium ion batteries. J. Power Sources 2014, 248, 1211 1217.

(15) Zhao, Q.; Yang, D.; Whittaker, A. K.; Zhao, X. S. A hybrid sodium-ion capacitor with polyimide as anode and polyimide-derived carbon as cathode. J. Power Sources 2018, 396, 12 18.

(16) Bell, V. L.; Stump, B. L.; Gager, H. Polyimide structure-property relationships. II. Polymers from isomeric dianhydrides. J. Polym. Sci., Polym. Chem. Ed. 1976, 14, 2275 2291.

(17) Fang, Q.; Zhuang, Z.; Gu, S.; Kaspar, R. B.; Zheng, J.; Wang, J.; Qiu, S.; Yan, Y. Designed synthesis of large-pore crystalline polyimide covalent organic frameworks. Nat. Commun. 2014, 5, No. 4503.

(18) Xue, J.; Wu, T.; Dai, Y.; Xia, Y. Electrospinning and Electrospun Nanofibers: Methods, Materials, and Applications. Chem. Rev. 2019, 119, 5298 5415.

(19) Yuan, K.; Guo-Wang, P.; Hu, T.; Shi, L.; Zeng, R.; Forster, M.; Pichler, T.; Chen, Y.; Scherf, U. Nanofibrous and Graphene-Templated Conjugated Microporous Polymer Materials for Flexible Chemoensors and Supercapacitors. Chem. Mater. 2015, 27, 7403 7411.

(20) Xiao, Y.; Huang, J.; Xu, Y.; Zhu, H.; Yuan, K.; Chen, Y. Hierarchical 1D nanofiber-2D nanosheet-shaped self-standing membranes for high-performance supercapacitors. J. Mater. Chem. A 2018, 6, 9161 9171.

(21) Jiang, S.; Helfricht, N.; Papastavrou, G.; Greiner, A.; Agarwal, S. Low-Density Self-Assembled Poly(N-Isopropyl Acrylamide) Sponges with Ultrahigh and Extremely Fast Water Uptake and Release. Macromol. Rapid Commun. 2018, 39, No. 1700838.

(22) Loubière, K.; Hérard, G. Influence of liquid surface tension (surfactants) on bubble formation at rigid and flexible orifices. Chem. Eng. Process. 2004, 43, 1361 1369.

(23) Cheong, J. Y.; Benker, L.; Zhu, J.; Youn, D.-Y.; Hou, H.; Agarwal, S.; Kim, I.-D.; Greiner, A. Generalized and feasible strategy to prepare ultra-porous, low density, compressible carbon nanoparticle sponges. Carbon 2019, 154, 363 369.

(24) Wang, C. W.; Wang, D.; Tang, Q. Effect of sodium dodecyl benzene sulfonate on the process of Fenton degradation of 4-chlorophenol. Desalin. Water Treat. 2015, 55, 1302 1307.

(25) Munirathnam, K.; Nagajyothi, P. C.; Prakashbbu, D.; Deva Prasad Raju, B.; Shim, J. X-ray photoelectron spectroscopy and optical analysis of pure white light emitting Dy^{3+} and Mn^{2+} codoped $NaY(PO_4)_2$ phosphors for solid-state lighting. Ceram. Int. 2019, 45, 686 694.

(26) She, Z. W.; Sun, J.; Sun, Y.; Cui, Y. A Highly Reversible Room-Temperature Sodium Metal Anode. ACS Cent. Sci. 2015, 1, 449 455.

(27) Thijs, H. M. L.; Becer, C. R.; G-Sanchez, C.; Fournier, D.; Hoogenboom, R.; Schubert, U. S. Water uptake of hydrophilic polymers determined by a thermal gravimetric analyzer with a controlled humidity chamber. J. Mater. Chem. 2007, 17, 4864 4871.

(28) Duan, G.; Jiang, S.; Jérôme, V.; Wendorff, J. H.; Fathi, A.; Uhm, J.; Altstädt, V.; Herling, M.; Breu, J.; Freitag, R.; Agarwal, S.; Greiner, A. Ultralight, soft polymer sponges by self-assembly of short electrospun fibers in colloidal dispersions. Adv. Funct. Mater. 2015, 25, 2850 2856.

(29) Kaiser, P.; Reich, S.; Leykam, D.; W-Porada, M.; Greiner, A.; Freitag, R. Electrogenic Single-Species Biocomposites as Anodes for Microbial Fuel Cells. Macromol. Biosci. 2017, 17, No. 1600442.

(30) Bullen, R. A.; Arnot, T. C.; Lakeman, J. B.; Walsh, F. C. Biofuel cells and their development. Biosens. Bioelectron. 2006, 21, 2015 2045.

(31) Yang, X.-Y.; Tian, G.; Jiang, N.; Su, G.-L. Immobilization technology: a sustainable solution for biofuel cell designy. Energy Environ. Sci. 2012, 5, 5540 5563.

(32) Hatakeyama-Sato, K.; Wakamatsu, H.; Katagiri, R.; Oyaizu, K.; Nishide, H. An Ultrahigh Output Rechargeable Electrode of a Hydrophilic Radical Polymer/Nanocarbon Hybrid with an Exceptionally Large Current Density beyond 1 A/cm^2. Adv. Mater. 2018, 30, No. 1800900.

(33) Koshika, K.; Sano, N.; Oyaizu, K.; Nishide, H. An Aqueous, Electrolyte-Type, Rechargeable Device Utilizing a Hydrophilic Radical Polymer-Cathode. Macromol. Chem. Phys. 2009, 210, 1989 1995.

(34) Zhao, C.; Lv, J.; Xu, X.; Zhang, G.; Yang, Y.; Yang, F. Highly antifouling and antibacterial performance of poly(vinylidene fluoride) ultrafiltration membranes blending with copper oxide and graphene oxide nanofillers for effective wastewater treatment. J. Colloid Interface Sci. 2017, 505, 341 351.

https://dx.doi.org/10.1021/acsami.0c03103
ACS Appl. Mater. Interfaces 2020, 12, 18002 18011

(35) Ma, S.; Chiu, C. P.; Zhu, Y.; Tang, C. Y.; Long, H.; Qarony, W.; Zhao, X.; Zhang, X.; Lo, W. H.; Tsang, Y. H. Recycled waste black polyurethane sponges for solar vapor generation and distillation. Appl. Energy 2017, 206, 63 69.
(36) Xue, G.; Xu, Y.; Ding, T.; Li, J.; Yin, J.; Fei, W.; Co, Y.; Yu, J.; Yuan, L.; Gong, L.; Chen, J.; Deng, S.; Zhou, J.; Guo, W. Water-evaporation-induced electricity with nanostructured carbon materials. Nat. Nanotechnol. 2017, 12, 317 321.
(37) Mader, M.; Jerome, V.; Freitag, R.; Agarwal, S.; Greiner, A. Ultraporous, compressible, wettable polylactidepolycaprolactone sponges for tissue engineering. Biomacromolecules 2018, 19, 1663 1673.
(38) Gao, Y.; Wang, J.; Mou, X.; Cai, Z. Textile-inspired methodology toward asymmetric fabric based on weft-backed weave for oil/water separation. J. Mater. Sci. 2018, 53, 4683 4692.
(39) Zhang, S.; Guo, J.; Ma, X.; Peng, X.; Qiu, Z.; Ying, J.; Wang, J. Smart PDMS sponge with switchable pH-responsive wetting surface for oil/water separation. New J. Chem. 2017, 41, 8940 8946.

https://dx.doi.org/10.1021/acsami.0c03103
ACS Appl. Mater. Interfaces 2020, 12, 18002 18011